JOURNAL OF CATALYSIS 143, 499–509 (1993)

Structure of a Nanophase Iron Oxide Catalyst

J. ZHAO, F. E. HUGGINS, ZHEN FENG, FULONG LU, NARESH SHAH, AND G. P. HUFFMAN[1]

Consortium for Fossil Fuel Liquefaction Science, 233 Mining and Mineral Resources Building, University of Kentucky, Lexington, Kentucky 40506

Received February 19, 1993; revised May 10, 1993

Iron *K*-edge X-ray absorption fine structure (XAFS) studies have been carried out to determine the bulk and surface structures of a nanophase iron oxide catalyst with average particle size of 30 Å. Both the extended X-ray absorption fine structure (EXAFS) and the X-ray absorption near-edge structure (XANES) spectra indicate that the structure of the catalyst is similar to iron oxyhydroxide. The intensity of the $1s \rightarrow 3d$ transition peak in the XANES of the 30-Å catalyst is increased by a factor of 1.7 compared with that for iron oxide and iron oxyhydroxide model compounds, in which iron ions are coordinated by six oxygens or oxygen/hydroxyl groups. The increase of the $1s \rightarrow 3d$ transition intensity is attributed to coordination unsaturated (CUS) sites on the particle surface produced by dehydroxylation. The absorption edge position of the 30-Å catalyst indicates that the valence state of the iron ions remains +3.

I. INTRODUCTION

In recent years, there has been extensive investigation of the use of iron-based catalysts for direct coal liquefaction (DCL) (*1–4*). The cost of iron-based catalysts is low, and disposal of the catalyst after reaction is unlikely to cause a significant environment hazard. Efforts have been made to produce highly dispersed catalysts so as to increase the surface area and decrease catalyst loading.

Recently, a highly dispersed iron oxide catalyst has been tested for DCL (*4, 5*). The catalyst (described as 30-Å catalyst in the following) is manufactured by Mach I, Inc. (NANOCAT, U.S. patent 5,047,382), and has been used in rocket propellants. The phase was identified as α-Fe_2O_3 by the manufacturer. The X-ray diffraction pattern (*6*) of this catalyst shows two very broad peaks corresponding to d = 2.63 and 1.50 Å. The Mössbauer spectrum of the catalyst recorded at 10 K shows a distribution of magnetic hyperfine splitting ranging from 440 to 507 kOe (*7*). These parameters are similar to those previously reported for ferrihydrite (*8*) and an amorphous FeOOH catalyst (*9*). Ferrihydrite is a naturally occurring hydrous iron oxide and is the initial precipitate that results from rapid hydrolysis of Fe(III) solution. It is a precursor of numerous other iron oxides and iron oxyhydroxides (*8*). Although the properties of ferrihydrite have been studied extensively, mainly by mineralogists, the basic structure of the material is still unclear. Several formulae have been proposed, e.g., $5Fe_2O_3 \cdot 9H_2O$, $Fe_5HO_8 \cdot 4H_2O$, and $Fe_6(O_4H_3)_3$ (*8*). The amorphous FeOOH catalyst, prepared by a procedure similar to that for ferrihydrite, is found to be very active and selective in the oxidative dehydrogenation of butene (*9*).

X-ray absorption fine structure (XAFS) spectroscopy provides a unique opportunity to determine the structure of nanophase systems with short-range order, such as catalysts (*10*). Analysis of the extended part of X-ray absorption fine structure (EXAFS) provides the identity, interatomic distances, and coordination numbers of atoms in the neighboring atomic shells surrounding the

[1] To whom correspondence should be addressed.

0021-9517/93 $5.00

central absorbing atom. For transition metal compounds with incompletely filled *d*-shell, small pre-edge peaks in the X-ray absorption near-edge structure (XANES) region have been assigned to the $1s \rightarrow 3d$ transition (*11–14*). The intensity of the transition is very sensitive to coordination symmetry. For iron oxides, the $1s \rightarrow 3d$ peak intensity of the iron *K*-edge XANES is governed by the average coordination number (N_{ave}) and the symmetry of oxygen anions coordinating the central iron cation (*14*). This pre-edge peak has been successfully used to interpret the valence state and coordination of high-T_c superconductors (*15*), amorphous materials (*16, 17*), and protein complexes (*14*). In this investigation, the structure of the 30-Å catalyst is characterized by analyzing its EXAFS and XANES spectra. Because the catalyst particle size is unusually small, it is also possible to extract structural information for the surface iron ions from the spectra.

II. EXPERIMENTAL

The 30-Å catalyst is a free flowing powder of reddish-brown color with surface area greater than 250 m^2/g. It is very sensitive to moisture. According to the manufacturer, the sample may absorb as much as 15% by weight of water upon prolonged exposure to the atmosphere, although it can be redried in a few hours at 150°C in vacuum. The sample, which was shipped to us in a sealed tin, was repacked in small bottles or plastic bags in a glove box filled with N_2 gas to avoid unnecessary exposure to moisture.

The morphology of the sample was investigated by transmission electron microscopy (TEM) with a Hitachi H800 NA scanning transmission electron microscope.

Iron *K*-edge X-ray absorption spectra were collected at the National Synchrotron Light Source (NSLS) on beam line X-19A at Brookhaven National Laboratory. The radiation was monochromatized with a Si(111) double-crystal monochromator with energy resolution ~1 eV at Fe *K*-edge. The monochromator was detuned by 60% to reduce the harmonic content. The data were collected in the transmission mode with two ion chambers for recording I and I_0 respectively. The X-ray energy was varied from 100 eV below to 1000 eV above the Fe *K*-edge at 7112 eV. The zero energy point for the Fe *K*-edge was defined as the first inflection point of the XAFS spectrum of α-iron foil. The XANES region of the spectra was measured in 0.2-eV steps.

The samples investigated included an as-received sample, a moist-air-exposed sample, and several model compounds. The model compounds were laboratory synthesized and characterized by XRD. Samples for the XAFS experiments were prepared by uniformly spreading fine sample powder on a thin tissue paper and sealed by Scotch tape. Precautions were taken to avoid thickness effects which can cause distortion of the XAFS scattering amplitude. For each sample, 3–4 samples of different thicknesses were prepared for XAFS measurements and the spectra with negligible thickness effects were chosen for detailed analysis. All spectra were collected at liquid-nitrogen temperature, unless otherwise noted.

III. EXAFS DATA ANALYSIS

Standard procedures were followed for EXAFS data analysis (*10*). Parameterized scattering amplitude $F(k)$ and scattering phase shift $\varphi(k)$ (*18*) were first calculated by fitting the spectrum of a model compound with known coordination number (N) and interatomic distance (R). These parameters were then used as constants to fit the sample spectra to obtain the structural parameter N, R, and σ^2 for the samples. γ-FeOOH was used as a primary standard. Its EXAFS radial structure function (RSF), which is the Fourier transform of the EXAFS spectrum, $\chi(k)$, is shown in Fig. 1a. For comparison, a radial distribution function (RDF), calculated from the X-ray crystallographic data (*19*) using the program SEXIE (*20*), is shown in Fig. 1b. The EXAFS RSF for γ-FeOOH exhibits a strong peak at 2.75 Å (Fig. 1a)

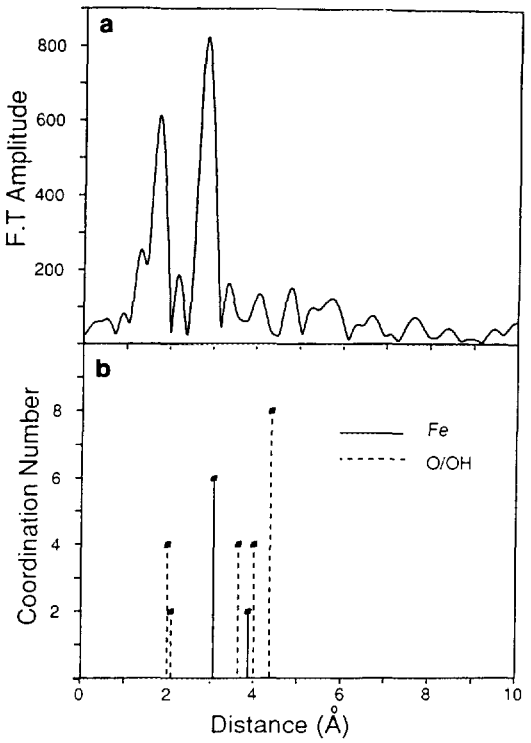

FIG. 1. (a) EXAFS RSF for γ-FeOOH and (b) RDF for γ-FeOOH calculated from X-ray crystallographic data.

that represents an iron shell at 3.05 Å with coordination number $N = 6$ (Fig. 1b). The shift of peak position in the EXAFS RSF is due to the scattering phase shift $\varphi(k)$. This iron shell is well separated from neighboring shells at 2.066 ($N_{oxy} = 2$), 3.62 ($N_{oxy} = 6$), and 3.87 Å ($N_{Fe} = 2$). Therefore it is an ideal standard Fe shell. For the O/OH shells, the nearest O/OH shell(s) of γ-FeOOH at an average distance of 2.01 Å and $N = 6$ (peak at ~1.60 Å in Fig. 1a) was used as the O/OH shell standard. It represents three O/OH shells at 1.975 ($N = 2$), 1.993 ($N = 2$), and 2.066 Å ($N = 2$).

For the samples, a two-shell model was used for fitting the nearest O/OH shells and 2–4 shell models for fitting the iron shells. The approximate resolving power of EXAFS for two shells of the same atomic type is $\Delta r = \pi/2k_{max}$ (*21*). Since k_{max} for the current EXAFS data is about 14–15 Å^{-1}, $\Delta r = 0.1$ Å. This resolving power also depends on the noise level and the type of the scatterers. Teo *et al.* (*18*) showed that for scatterers with atomic number $Z < 36$, the scattering amplitude $F_i(k)$ can be approximated by a Lorentzian function,

$$F(k) = \frac{A}{1 + B^2(k - C)}. \quad (1)$$

For an iron scatterer, $A = 0.679$, $B = 0.1939$, and $C = 6.355$ Å^{-1} (*18*), and therefore at $k = 10$ and 15 Å^{-1}, F_{Fe} reduces to 0.453 and 0.178, respectively. However, for an oxygen scatterer, $A = 1.079$, $B = 0.4096$, and $C = 0.876$ (*18*), and therefore at $k = 10$ and 15 Å^{-1}, $F_{oxy} = 0.09$ and 0.049, respectively, which are much smaller than the corresponding values for iron. Noise in the data limits the effective k_{max} for oxygen to approximately 10 Å^{-1}, which constrains the effective resolving power for the oxygen shells to be 0.15–0.2 Å. Therefore, the uncertainty of the EXAFS analysis for oxygen shells is much larger than that for iron shells. Fortunately, accurate structural information about the nearest O/OH shells can be determined from the pre-edge structure in XANES, as discussed in detail later in this paper. For all the EXAFS spectra, the k^3 weighted Fourier transform $\chi(k)$ was taken at $k = 3.0$ to 14.0 Å^{-1} and least-squares fitting of the inverse Fourier transform spectrum was carried out over the range $k = 3.5$ to 13.5 Å^{-1}.

IV. RESULTS AND DISCUSSION

Morphology of the Samples

Figure 2 shows the electron micrograph and microdiffraction of the 30-Å catalyst. The particle size distribution is shown in Fig. 3. Since the particle size is comparable to the electron beam size (~50 Å), only rings are observed in the electron diffraction pattern.

EXAFS Results

The parameterized phase shift $\varphi(k)$ and amplitude $F(k)$ extracted from the γ-

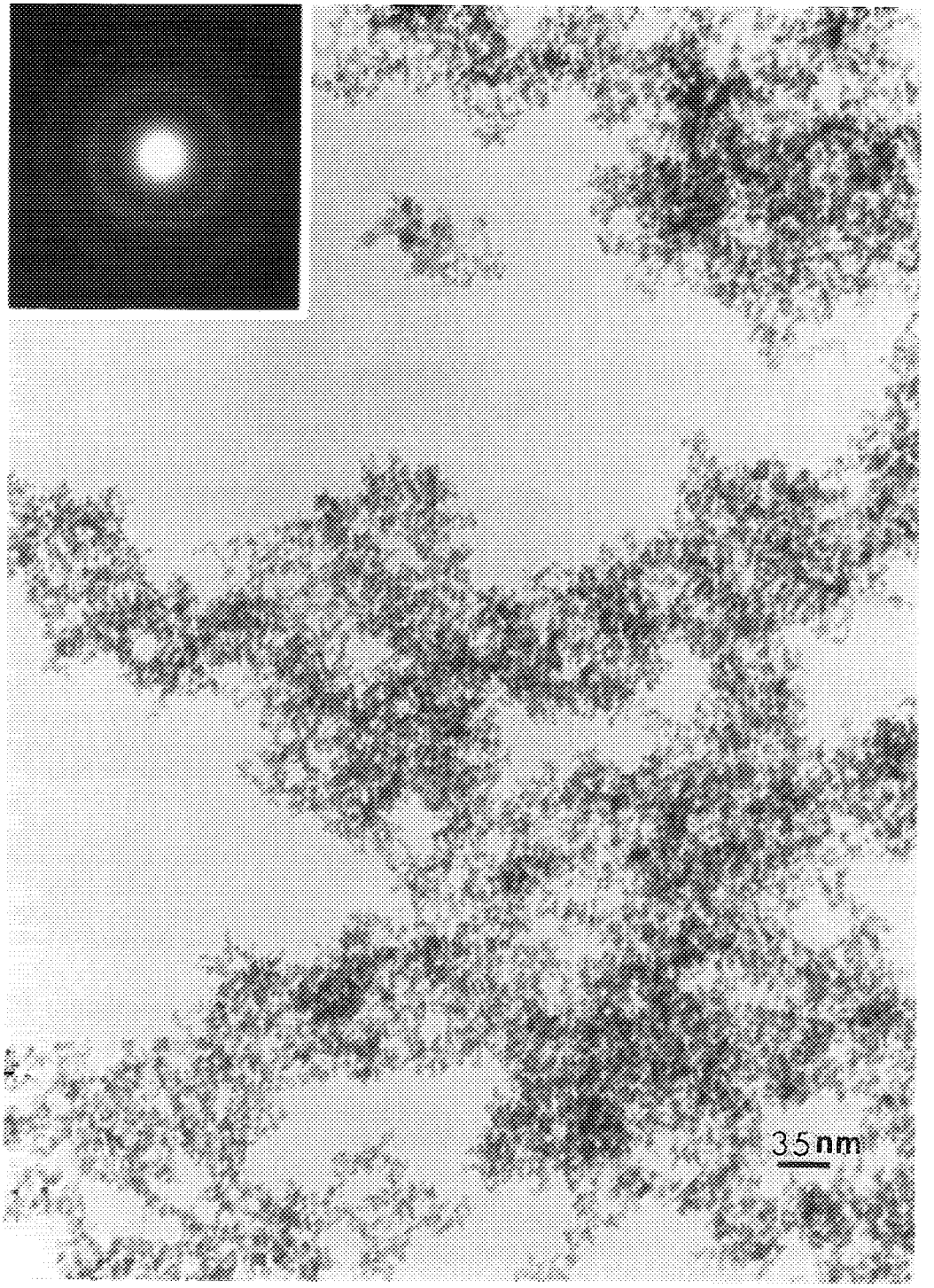

FIG. 2. Electron micrograph and electron micro-diffraction (inset) for the 30-Å catalyst.

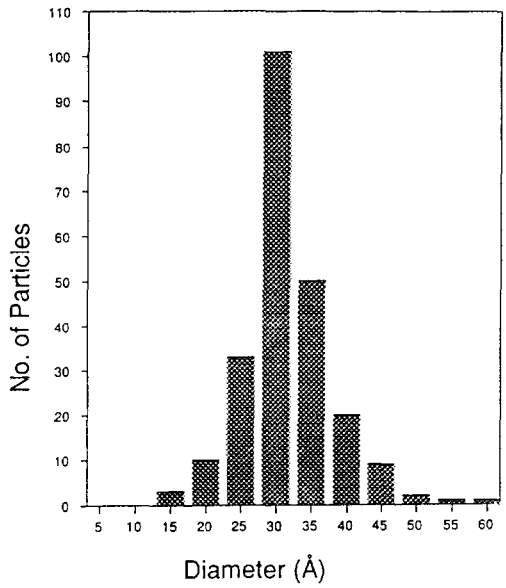

FIG. 3. Size distribution of the 30-Å catalyst.

FeOOH iron shell were first used to fit the Fe/O shells for α-Fe_2O_3. Two distinct peaks from 2.3–4.0 Å are observed in the α-Fe_2O_3 RSF (Fig. 4a). These two peaks actually represent four iron shells and three oxygen shells (Fig. 4b). To simplify the calculation, this region was modeled with only three iron shells. Since the oxygen shell contribution is mainly in the low-k region (*22*), the amplitude function $F(k)$ obtained from γ-FeOOH was modified to make $F(k)$ broad by decreasing the B-value in Eq. (1) and centered at lower k region by decreasing C-value in Eq. (1), so as to include the scattering amplitude from the oxygen shells. Thus a new scattering amplitude $F'(k)$ was generated and used for fitting the second and the third Fe shell of α-Fe_2O_3. $F(k)$ was used for the first Fe shell of α-Fe_2O_3. Depending on the specific structures of the sample, $F(k)$ and/or $F'(k)$ was used to fit the spectra of other model compounds and the catalyst samples.

The least-squares fitting results for the Fe/O shells are listed in Table 1. The coordination numbers in Table 1 were normalized with respect to the coordination numbers for the three Fe shells of α-Fe_2O_3. In comparison with the interatomic distances calculated from crystal structures (*19*), the estimated errors for the interatomic distances are less than 0.04 Å. Larger errors were found in the coordination numbers, which can be attributed to the different chemical environments of the compounds (*23*). For the 30-Å catalyst, the spectrum was fitted with both a two-shell model and a one-shell model (Fig. 5); it can be seen that the two shell model gives the better fit to the spectrum and reasonable structural parameters (Table 1). The first Fe shell at R_1 = 3.00–3.01 Å is similar to that for iron oxyhydroxides at R_1 = 3.01–3.05 Å, but it is larger than that for iron oxides at R_1 = 2.92–2.95 Å. The RSF of the 30-Å catalyst compared to those for various model compounds is shown in Fig. 6. It can be readily seen that the position of the first Fe shell for the 30-Å catalyst is closer to that for oxyhydroxides.

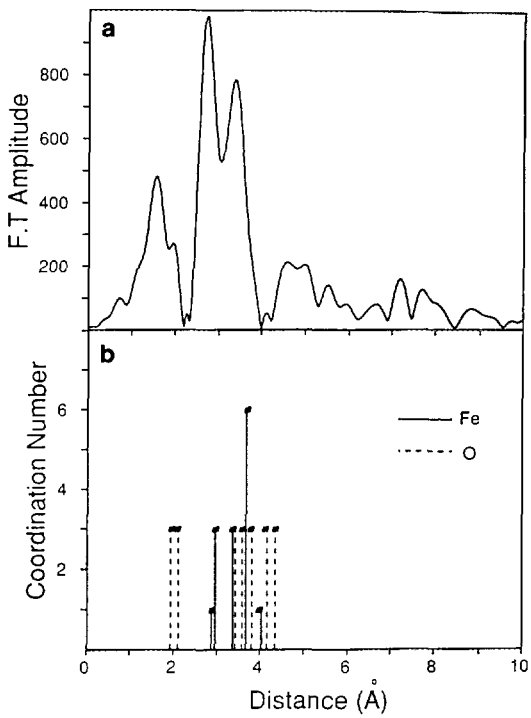

FIG. 4. (a) EXAFS RSF for α-Fe_2O_3 and (b) RDF for α-Fe_2O_3 calculated from X-ray crystallographic data.

TABLE 1

Structural Parameters of the Nearest Iron Shells for the Catalyst Samples Iron Oxide, and Iron Oxyhydroxide model compounds

Sample	Distance (Å)	Coordination number	$\Delta\sigma^2$	Inverse FT range (Å)
α-Fe_2O_3	2.95 (2.95)	(4)	0.0	2.2–4.0
	3.36 (3.37)	(3)	0.0	
	3.70 (3.70)	(6)	0.0	
Fe_3O_4	2.93 (2.97)	2.8 (4)	+0.0028	2.2–3.6
	3.44 (3.48)	5.2 (8)	+0.0026	
	(3.64)	(1.3)		
γ-Fe_2O_3	2.94	1.8	+0.004	2.3–3.6
(Room temp.)	3.39	4.5	+0.0029	
α-FeOOH	3.02 (3.03)	1.8 (2)	−0.0016	2.2–3.7
	3.40 (3.44)	2.6 (6)	+0.0054	
γ-FeOOH	3.05 (3.05)	6.0 (6)		2.3–3.3
(As standard)				
30-Å, fresh	3.01	1.4	+0.0008	2.5–3.3
(Two-shell fit)	3.12	0.6	−0.0022	
(One-shell fit)	3.08	2.5	+0.0064	2.5–3.3
30-Å	3.00	1.2	+0.0008	2.5–3.3
(Air-exposed)	3.14	0.7	−0.0007	

Note. Values in the parentheses are calculated from the X-ray crystallographic data (*19*). $\Delta\sigma^2$ is the relative D–W factor as compared with that for α-Fe_2O_3.

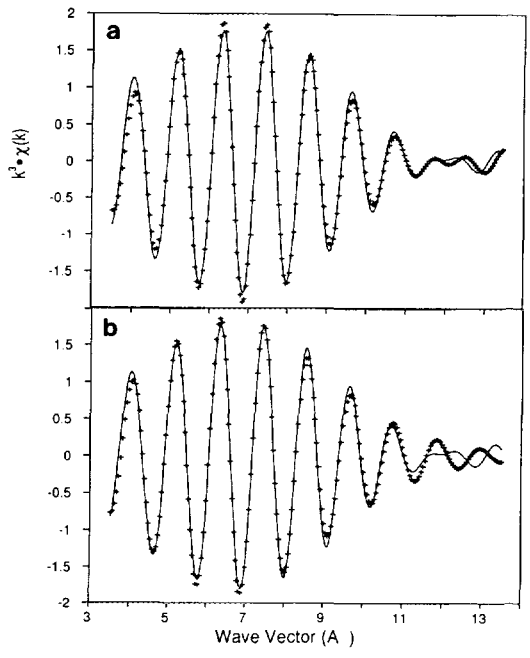

FIG. 5. Least-squares analysis of the inverse Fourier transform of the iron shell(s) for the 30-Å catalyst: (a) two-shell fitting and (b) one-shell fitting.

The second iron shell at 3.12 Å for the 30-Å catalyst does not fit with any iron shell distance in the model compounds. This distance may represent the variation of the Fe–Fe distances near the particle surface. For samples with particles of size >100 Å, the EXAFS signals from surface atoms are not detectable because the surface constitutes an insignificant fraction (<10%) of the sample. However, for a 30-Å particle, if we consider that the surface is a 2-Å layer (equivalent to the O–Fe distance), as many as 35% of the atoms of the particle can be considered to be surface atoms which makes the observation of the surface structure possible.

EXAFS least-squares fitting results of the oxygen shells are listed in Table 2. The average coordination number of the 30-Å catalyst is 5.5 and its average Fe–O distance 2.00 Å. These values are slightly less than those for γ-FeOOH, α-FeOOH, and α-Fe_2O_3 (N = 6 and R > 2.01 Å), and close to those for Fe_3O_4 (N = 5.3, R = 2.00 Å)

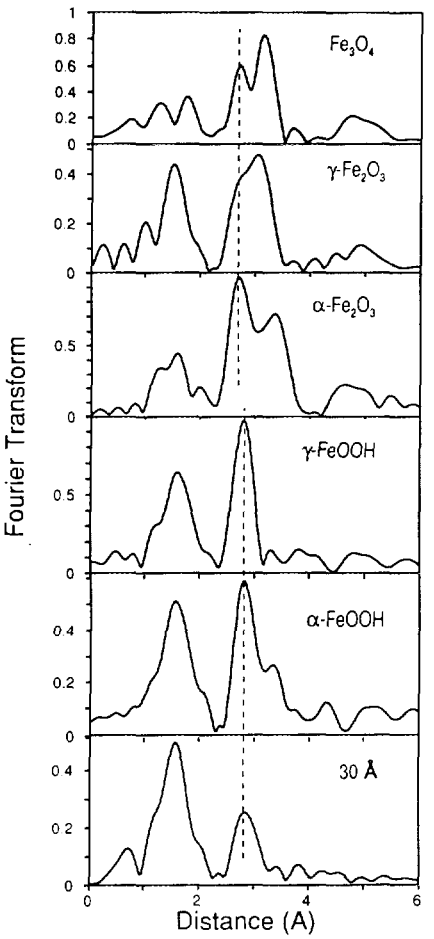

FIG. 6. EXAFS RSF's for the 30-Å catalyst and model compounds.

and γ-Fe_2O_3 ($N = 5.5$ and $R = 2.00$ Å) (Table 2). However, the differences are still within the errors of EXAFS analysis.

For the 30-Å catalyst, both the fitting results (Tables 1 and 2) and the RSF (Fig. 6) indicate that the coordination number of the nearest O/OH shell(s) remains approximately the same as that for the model compounds, but that the coordination numbers of the iron shells decrease substantially. This is attributed to the fact that the iron atoms on the particle surface have about half as many iron neighbors as iron atoms in the bulk, and as the particle size decreases, the percentage of surface iron ions increases, the average iron shell coordination number for small particles decreases. However, these surface iron ions may continue to have close to the full complement of surrounding oxygen/hydroxyl groups, since the sample is an oxide and the outermost layer of the particle consists of either oxygens or hydroxyl groups (*24*).

XANES Results

The X-ray absorption near edge structure (XANES) is a result of multiple scattering resonances (*25*) and is often used as a fingerprint for phase identification. The Fe-edge XANES spectra for the 30-Å catalyst and several model compounds are shown in Fig. 7. The iron ions in oxyhydroxides are coordinated on average by three oxygen and three hydroxyl groups. Their XANES spectra are similar to each other. The iron ions in α-Fe_2O_3 are surrounded by six oxygens; the XANES spectrum shows three distinct peaks (labeled as a, b, and c in the figure). Because some of the iron ions are at the tetrahedral sites, there is an obvious change in the XANES for Fe_3O_4 and γ-Fe_2O_3 compared to that for α-Fe_2O_3. The XANES spectrum for the 30-Å catalyst is similar to those of the iron oxyhydroxides. Therefore, both EXAFS and XANES results indicate that the structure of the 30-Å catalyst is oxyhydroxide like.

The XANES spectra for iron oxides usually exhibit a small pre-edge peak below the midpoint of the absorption edge, which is assigned to $1s \rightarrow 3d$ transitions, and a main peak corresponding to transitions from $1s$ to unfilled $4p$ states. For K-edge absorption, dipole selection rules allow transitions from the initial $1s$ state to final p states, only. However, hybridization of d and p states can make the $1s$ to nd state transition possible. Using molecular-orbital theory, Roe *et al.* (*14*) found a reasonable correlation of the pre-edge intensity with the total amount of iron $4p$ orbital mixed into the predominantly $3d$ orbital. The ratio of the peak areas for iron ions with six neighbors, five neighbors,

TABLE 2

Structural Parameters of the Nearest Oxygen/Hydroxyl Shells and Fe Pre-edge Structure Features for the Catalyst Samples and Model Compounds.

Compound	Formal valence	Bond type	Number of coordinates	Ave. distance		$\Delta\sigma^2$	Peak area $1s$–$3d$ trans. ($\Delta < \pm 0.01$)
FeO	2	Fe–O	(6)		(2.16)		0.043
γ-FeOOH	3	Fe–OH/O	(6)		(2.01)		0.068
α-FeOOH	3	Fe–OH/O	(6)		(2.08)		0.077
α-Fe_2O_3	3	Fe–O	(6)	2.03	(2.03)		0.074
Fe_3O_4	2.7	Fe–O	(5.3)		(2.00)		0.141
γ-Fe_2O_3	3	Fe–O	(5.5)		(2.00)		0.126
30-Å, fresh		Fe–O/OH	5.5	1.99		0.0011	0.127
30-Å (air-exposed)		Fe–O/OH	5.5	2.01		0.0011	0.110

Note. Values in the parentheses are calculated from X-ray crystallographic data (*19*). $\Delta\sigma^2$ is the relative D–W factor as compared with that for α-Fe_2O_3.

and 4 neighbors is found to be 1 : 2 : 3 (*14*). The d orbital of a transition metal ion split into e_g and t_{2_g} groups in an octahedral crystal field or t_2 and e groups in a tetrahedral crystal field. For oxygen ligands, the splitting for the e_g and t_{2_g} orbital, Δ_{oct}, is found to be ~1.5 eV, and the splitting for the t_2 and e orbital, $\Delta_{tetr} = (4/9) \cdot \Delta_{oct} = 0.7$ eV (*26*).

Figure 8 shows the pre-edge structures of several iron model compounds and the 30-Å catalyst. The pre-edge structures were least-squares fitted from −6 to 12 eV with an arctangent function representing the absorption background and three Lorentzian peaks. Two major peaks with width of ~1.6 eV are assigned to $1s \rightarrow 3d$ transitions. The origin of the third broad peak on the high energy side of these two peaks is unknown (Fig. 9). The heights of the peaks were normalized with respect to the edge step height. The areas of the $1s \rightarrow 3d$ peaks, determined by multiplying the peak heights by the peak widths at 1/2 height, are summarized in Table 2. FeO exhibits very small $1s \rightarrow 3d$ transition peak areas (0.043 unit) because it contains regular octahedral FeO_6 units, with a center of inversion. As the octahedron units become more distorted, the inversion symmetry may disappear, as in the case of γ-FeOOH, α-FeOOH, δ-FeOOH, and α-Fe_2O_3, and the peak area increases by almost a factor of 2, to 0.068–0.077 unit. The splitting of the two peaks of these samples is about 1.3–1.4 eV. For γ-Fe_2O_3 and Fe_3O_4, which have 25 and 33% of the iron ions at tetrahedral sites, the $1s \rightarrow 3d$ peak area increases to 0.126 and 0.141 unit, respectively, and the splitting of the two peaks decreases to 0.9 (γ-Fe_2O_3) and 1.0 eV (Fe_3O_4). For the 30-Å catalyst, although both EXAFS and XANES results indicate an FeOOH structure, the $1s \rightarrow 3d$ transition peak area is 0.127 unit and the splitting of the two peaks is 0.9 eV, suggesting that as much as 25% of the iron ions may be coordinated by four oxygens/hydroxyl groups, assuming tetrahedral symmetry. This change of the pre-edge peak area is unlikely to be due to the defects or disorder in the material. As summarized by Roe *et al.* (*14*), the variation in pre-edge area due to bond distance change is in the range of 0.01 unit, which is much smaller than that reported in this work (0.05 unit). In the past, variation of the pre-edge peak intensity of this scale has always been attributed to the change of coordination symmetry (*11, 13–17*).

The XANES features of the 30-Å catalyst suggest that the lower coordinated sites are on the particle surface. The phenomenon of

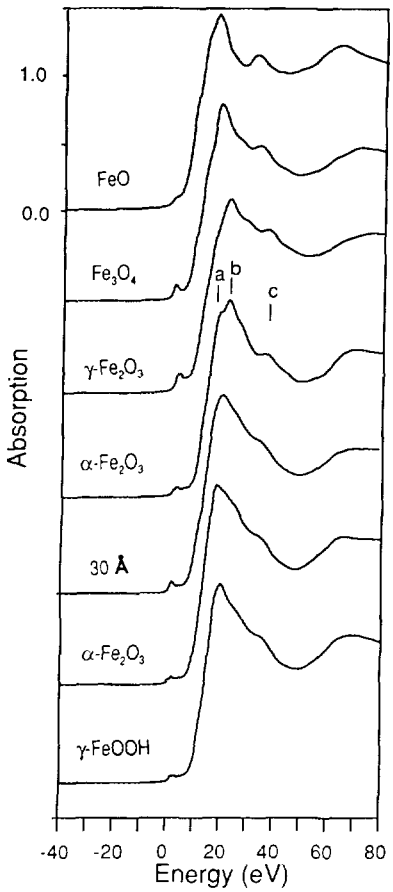

FIG. 7. XANES for the 30-Å catalyst and model compounds.

XANES can be understood as a "cluster effect" (*11*, *25*) which is a result of multiple scattering resonances of the outgoing photoelectron from the absorbing atom at the center of the cluster with the atoms in neighboring shells. Theoretical calculation by Greaves *et al.* (*25*) demonstrated that only a cluster with at least three or more shells shows distinct near-edge features in agreement with observation. For the surface atoms, with neighboring atoms on the bulk side only, the number of possible multiple scattering pathways is greatly reduced. Therefore, the conditions for multiple scattering resonance do not exist for surface atoms. In other words, the environment of the absorbing atoms in the bulk of the particle dominates the XANES spectra. As noted by Bianconi (*11*), the XANES features are determined by the geometrical distribution, that is, bond angles and relative atomic positions in the environment of the absorbing atom. If the sites with lower coordination were in the bulk of the particle, we would expect the XANES for the 30-Å catalyst (assuming 25% atoms at tetrahedral sites) to be significantly different from that for octahedral oxyhydroxides, similar to the difference between the XANES for γ-Fe_2O_3 and that for α-Fe_2O_3 (Fig. 7). However, this is not the case. As seen in Fig. 6, the XANES spectrum for the 30-Å catalyst closely resembles the XANES spectra for the octahedral oxyhydroxides. This similarity indicates that the lower coordination sites are on the particle surface.

These lower coordination sites appear to be coordination unsaturated. After exposure to air, the $1s \rightarrow 3d$ peak area decreased to 0.110 unit (Table 2), indicating an increase of average coordination number as a result of adsorbed water molecules at the surface of the catalyst. As discussed above, the pre-edge is very sensitive to

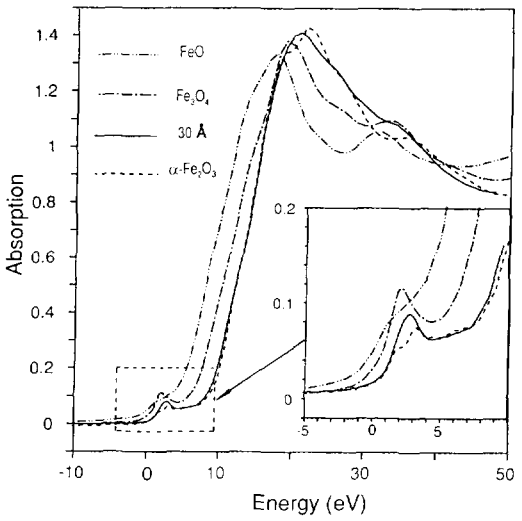

FIG. 8. XANES pre-edge structures for FeO, Fe_3O_4, α-Fe_2O_3, and the 30-Å catalyst.

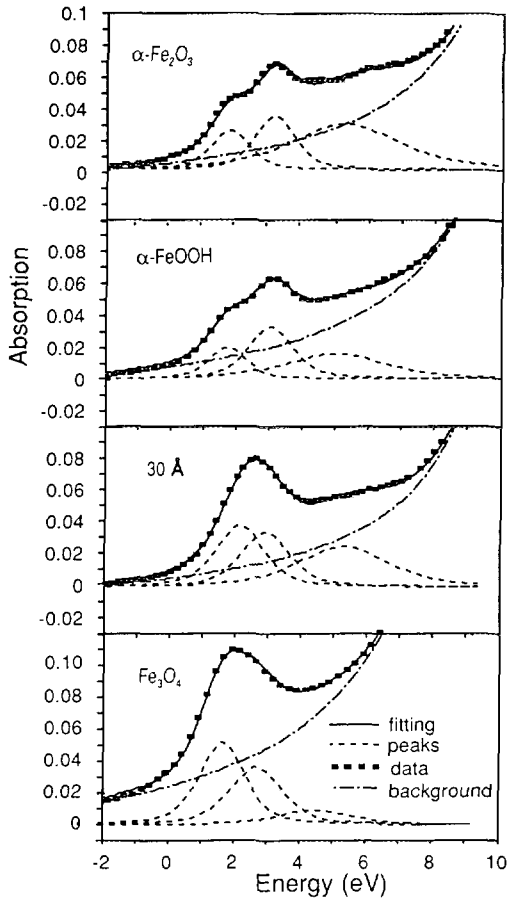

FIG. 9. Least-squares fitting of the XANES pre-edge feature for α-Fe_2O_3, α-FeOOH, the 30-Å catalyst, and Fe_3O_4.

the change of coordination symmetry. The decrease of the pre-edge area in the moist-air-exposed sample only corresponds to an increase of average coordination number of <0.2, a change that is too small to be detected by EXAFS analysis (Table 2), which has an uncertainty of 10–20% for coordination determination. The reduction in pre-edge area due to exposure to moisture has also been observed in different sample batches provided by March I, Inc., and in a ferrihydrite (*8*) sample synthesized in our lab (*27*).

The lower coordination number for the surface iron ions and the increase of coordination number as a result of moist air exposure are consistent with the presence of coordination unsaturated (CUS) sites at the oxide surface (*24*, *28*). These CUS sites are also known as Lewis acid sites produced by dehydroxylation. On the (111) surface of γ-Al_2O_3, as many as 50% of the surface Al ions may occupy CUS sites with three oxygen nearest neighbors (*24*). Much of the information about CUS sites or Lewis acid sites is currently obtained from the fundamental OH-stretching vibration in IR spectra (*24*, *28*). Our investigation of the 30-Å catalyst demonstrates that XAFS spectroscopy may also be used as an alternative probe for detecting surface CUS sites.

The energy shift of the absorption edge is known as the chemical shift because the edge shifts to positive energy with increasing formal valence. This can be conceptually understood as due to an increase in the attractive potential of the nucleus on the 1*s* core electron as the formal valence increases. The absorption edge position of the 30-Å catalyst indicates that the valence state of iron remains +3, compared with FeO (+2), Fe_3O_4 (+2.67), and α-Fe_2O_3 (+3) (Fig. 8).

The proposed structure of the 30-Å catalyst is shown in Fig. 10. The surface iron ions are assumed to have tetrahedral symmetry. The phase of the catalyst can be described as $FeOOH \cdot xH_2O$, where H_2O are the water molecules adsorbed on the surface and x depends on preparation and pretreatment conditions. Whereas the surface CUS site may be the active sites for dehydrogenation of butene (*9*), the exact role of these

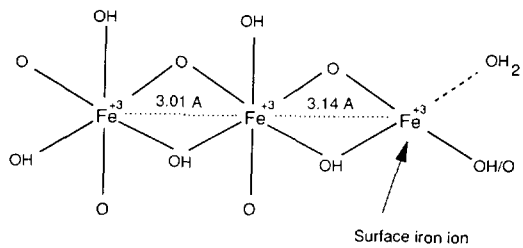

FIG. 10. Proposed structural model for the 30-Å catalyst.

CUS sites in direct coal liquefaction (DCL) is still unclear. It has been suggested that the presence of Lewis acid sites on the surface of the DCL active catalyst, Fe_2O_3/SO_4^{-2} may prevent particle agglomeration during calcination and DCL reaction (*4*). For the Fe_2O_3/SO_4^{-2} catalyst, CUS sites or Lewis acid sites are formed by introducing SO_4^{-2} groups to the Fe_2O_3 particle surface (*29*). In the following paper of this series (*30*), the effect of the surface structure and conditions on the phase transition and particle agglomeration of the 30-Å catalyst will be addressed.

ACKNOWLEDGMENTS

We are grateful to Dr. Bernard M. Kosowski of Mach I, Inc., 340 East Church Road, King of Prussia, PA 19406, who provided the 30-Å catalyst. This research is supported by the U.S. Department of Energy under Contract DE-FC22-90PC90029, as part of the research program of the Consortium for Fossil Fuel Liquefaction Science. The XAFS experiments were conducted at the National Synchrotron Light Source at Brookhaven National Laboratories, which is also supported by the U.S. Department of Energy.

REFERENCES

1. Derbyshire, F. J., *Energy Fuels* **3,** 273 (1989).
2. Pradhan, V. R., Tierney, J. W., Wender, I., and Huffman, G. P., *Energy Fuels* **5,** 497 (1991).
3. Taghiei, M. M., Huggins, F. E., Ganguly, B., and Huffman, G. P., *Energy Fuels* **7,** 399 (1993).
4. Huffman, G. P., Ganguly, B., Zhao, J., Rao, K. R. P. M., Shah, N., Feng, Z., Huggins, F. E., Taghiei, M. M., Lu, F., Wender, I., Pradhan, V. R., Tierney, J. W., Seehra, M. M., Ibrahim, M. M., Shabtai, J., and Eyring, E. M., *Energy Fuels* **7,** 285 (1993).
5. Farcasiu, M., personal communication.
6. Ibrahim, M. M., and Seehra, M. S., unpublished data.
7. Ganguly, B., Huggins, F. E., Feng, Z., and Huffman, G. P., submitted for publication.
8. Schwertmann, U., and Cornell, R. M., "Iron Oxides in the Laboratory." VCH, Weinheim, 1991, and references therein.
9. Liaw, B. J., Chen, D. S., and Yang, B. L., *J. Catal.* **118,** 312 (1989).
10. Prins, R., and Koningsberger, D. C., *in* "X-ray Absorption, Principles, Applications and Techniques of EXAFS, SEXAFS, and XANES" (D. C. Koningsberger and R. Prins, Eds.), p. 321, Wiley, New York, 1988.
Köningsberger and R. Prins, Eds.), p. 321, Wiley, New York, 1988.
11. Bianconi, A., *in* "X-ray Absorption, Principles, Applications and Techniques of EXAFS, SEXAFS, and XANES" (D. C. Koningsberger and R. Prins, Eds.), p. 573. Wiley, New York, 1988.
12. Schulman, R. G., Yafet, Y., Eisenberger, P., and Blumberg, W. E., *Proc. Natl. Acad. Sci. U.S.A.* **73,** 1384 (1976).
13. Wong, J., Lytle, F. W., Messmer, R. R., and Maylotte, D. H., *Phys. Rev. B* **30,** 5596 (1984).
14. Roe, A. L., Schneider, D. J., Mayer, R. J., Pytz, J. W., Widom, J., and Que, L., Jr., *J. Am. Chem. Soc.* **106,** 1676, (1984).
15. Yang, C. Y., Heald, S. M., Tranquada, J. M., Xu, Youwen, Moodenbaugh, A. R., Welch, D. O., and Suenaga, M., *Phys. Rev. B* **39,** 6681 (1989).
16. Calas, G., and Petiau, J., *Solid State Commun.* **48,** 625 (1983).
17. Combes, J. M., Manceau, A., and Calas, G., *Physica B* **158,** 419 (1989).
18. Teo, B. K., Lee, P. A., Simons, A. L., Eisenberger, P., and Kincaid, B. M., *J. Am. Chem. Soc.* **99,** 3854 (1977).
19. Wyckoff, R. W. G., "Crystal Structures," 2nd ed. Wiley, New York, 1968.
20. Program provided by Dr. Bernhard Rupp of Lawrence Livermore National Laboratory.
21. Teo, B. K., and Lee, P. A., *J. Am. Chem. Soc.* **101,** 2815 (1979).
22. Lee, P. A., Citrin, P. H., Eisenberger, P., and Kincaid, B. M., *Rev. Mod. Phys.* **53,** 769 (1981).
23. Eisenberger, P., and Lengeler, B., *Phys. Rev. B* **22,** 3551 (1980).
24. Knözinger, H., and Ratmasamy, P., *Catal. Rev.-Sci. Eng.* **17,** 31 (1978).
25. Greaves, G. N., Durham, P. J., Diaken, G., and Quinn, P., *Nature* **294,** 139 (1981).
26. Marfunin, A. S., "Physics of Minerals and Inorganic Materials," p. 59. Springer-Verlag, New York, 1974.
27. Zhao, J., Huggins, F. E., Feng, Z., and Huffman, G. P., unpublished data.
28. Kung, H., "Transition Metal Oxides: Surface Chemistry and Catalysts." Elsevier, Amsterdam, 1989.
29. Jin, T., Yamaguchi, T., and Tanabe, K., *J. Phys. Chem.* **90,** 4794 (1986).
30. Feng, Z., Zhao, J., Huggins, F. E., and Huffman, G. P., *J. Catal.*, **143,** 510 (1993).